Nano Today 40 (2021) 101270

Contents lists available at ScienceDirect

Nano Today

journal homepage: www.elsevier.com/locate/nanotoday

Scalable manufacturing of fibrous nanocomposites for multifunctional liquid sensing

Sheila M. Goodman[a], Ignacio Asensi Tortajada[b,c], Florian Haslbeck[b], Kaan Yüksel Oyulmaz[b,d], André Rummler[b], Carlos Solans Sánchez[b], Jose Torres País[c], Haluk Denizli[d], Kurt J. Haunreiter[a], Anthony B. Dichiara[a,*]

[a] School of Environmental & Forest Sciences, University of Washington, Seattle 98195, USA
[b] CERN, Esplanade des Particules 1, 1217 Meyrin, Switzerland
[c] Escuela Técnica Superior de Ingeniería, Universidad de Valencia, 46100 Burjassot, Spain
[d] Bolu Abant Izzet Baysal University, 14030 Merkez/Bolu, Turkey

ARTICLE INFO

Article history:
Received 27 April 2021
Received in revised form 22 July 2021
Accepted 10 August 2021
Available online 18 August 2021

Keywords:
Cellulose nanofibrils
Carbon nanotubes
Paper-based electronics
Liquid sensing
Leak detection

ABSTRACT

Cellulose-based paper electronics is an attractive technology to meet the growing demands for naturally abundant, biocompatible, biodegradable, flexible, inexpensive, lightweight and highly miniaturizable sensory materials. The price reduction of industrial carbon nanotube (CNT) grades offers opportunities to manufacture electrically conductive papers whose resistivity is responsive to environmental stimuli, such as the presence of water or organic solvents. Here, a highly sensitive paper nanocomposite is developed by integrating CNTs into a hierarchical network of pulp fibers and nanofibrillated cellulose. The aqueous-phase dynamic web forming process enables the scalable production of sensory paper nanocomposites with minimal nanoparticle loss due to the tailored interfacial bonding between CNT and cellulose components. The resulting materials are applied as multifunctional liquid sensors, such as leak detection and wave monitoring. The sensitivity to liquid water spans an outstanding four orders of magnitude even after 30 cycles and 6-month natural aging, due to the hydroexpansion of the hierarchical cellulose network, which alters the intertube distance between neighboring CNTs. The re-organization of percolated CNTs modifies the electron transport in wet areas of the sheet, which can be predicted by an equivalent circuit of resistors for the rapid detection and quantification of various liquids over large surfaces.

© 2021 Published by Elsevier Ltd.

Introduction

While a fifth of the world population lacks safe water, leaky pipes and wasteful irrigation systems are major contributors to water scarcity on the planet. The American Society of Civil Engineers indicates that about a quarter-million water line breaks occur each year in the U.S., representing more than 26 billion liters lost each day due to leaky pipes and costing public water utilities up to $2.8 billion annually [1]. In addition, 37% of U.S. homeowners are reported to have suffered losses from water damage, costing another $2.5 billion annually to insurance companies [2]. Worldwide, the World Bank estimates that global non-revenue water, which refers to the cost of water lost to leaks and billing errors approaches $14 billion. Although existing systems can detect and quantify the extent of water losses, they typically attempt to infer leak location *via* flow rate variations, a process which is time consuming and requires human intervention to confirm. An ideal leak monitoring system would consist of a low cost array of optimally spaced remote sensors to minimize the reaction time to patch a leak and power off sensitive instruments when necessary. However, sensing liquid water in a reliable and affordable way poses a major challenge. Existing technologies remain expensive and either have weak or slow responses to water due to the non-polar nature of the materials employed, or is partially soluble in water, like most polymer-based systems, which produce inconsistent signals due to material degradation in aqueous environments [3–8].

Given its bio-renewable and hygroscopic nature, cellulosic paper provides an excellent platform for building sustainable and affordable water sensors with superior performance. To date, most research has focused on hosting various types of electrodes onto the surface of paper using pencil drawing, inkjet printing, sputtering, and other forms of coating techniques [9–12]. These methods,

* Corresponding author.
E-mail address: abdichia@uw.edu (A.B. Dichiara).

https://doi.org/10.1016/j.nantod.2021.101270
1748-0132/© 2021 Published by Elsevier Ltd.

however, are characterized by the low accuracy and non-uniformity of the electrode films formed on the paper surface, which adversely affect device performance and reliability, besides making the fabrication process at large scale very challenging. In contrast to these efforts, we previously proposed to incorporate electrically conductive nanoparticles into the fibrous network prior to sheet formation, which offers greater control over the percolated network of fillers constituting electric paths in the material [13]. The present research describes the fabrication of electro-conductive papers by an easy-scale-up process involving the continuous-flow filtration of aqueous suspensions of wood pulp pre-adsorbed with cellulose nanofibrils (CNFs) and carbon nanotubes (CNTs) to form hierarchically structured fibrous mats, which are further dewatered by subsequent pressing and drying. A key element of our approach consists of a unique binding chemistry ensuring a strong adhesion between the nanoparticles and the pulp fibers even at high loading (*i.e.* up to 15 wt%). This allows the manufacturing of paper nanocomposites using a pilot-scale web former mimicking industrial papermaking conditions with minimal nanoparticle loss.

Results and discussion

Characterization of paper nanocomposites

Prior to pilot scale experiments, handsheets are prepared based on our previously reported procedure, as illustrated in Fig. 1a [13]. For comparison purposes, handsheets were prepared using different electrically conductive nanoparticles and their combinations (Fig. A1). Industrial grade hydroxyl-functionalized CNTs were selected over alternative fillers, such as helical CNTs (h-CNTs) and graphene nanoplatelets (GnPs), due to their relatively low cost (Table A1) and superior dispersion quality in aqueous CNF (Fig. A2a), contributing to more uniform sheet formation and enhanced sensing performance (Fig. A3). The resulting paper nanocomposites are mechanically flexible and robust with uniform electrical conductivity across the 16-cm diameter sheet. Electron microscopy confirms the even distribution of nanoparticles in the paper without significant aggregation despite loadings as high as 15 wt% (Fig. 1b). This is attributed to the presence of CNFs playing two roles: (*i*) that of a dispersing agent for the hydrophobic CNTs and (*ii*) that of an interfacial reinforcing agent between the CNTs and the pulp fibers. The former role can be ascribed to the polarization of electrons in the sp2 CNT lattice induced by the fluctuations of counter-ions on the surface of the TEMPO-oxidized CNFs [14], which promotes the colloidal stabilization of CNT:CNF complexes in water by means of electrostatic repulsion and steric hindrance, as shown by absorption spectroscopy (Fig. A2b). The latter role is evidenced by the red-shifts observed with the addition of CNT:CNF complexes in the graphitic D- and G-bands, respectively around 1350 and 1580 cm^{-1}, of the Raman spectra of papers, which are indicative of strong bonding interactions between CNTs and the cellulose components (Fig. 1c). The good interfacial properties are further confirmed by tape peeling tests, where the thickness and the in-plane electrical resistance of paper nanocomposites with 15 wt% CNTs decreased respectively by less than 1% and 2% on average after peeling (Fig. 1d). SEM images of the paper and adhesive sides captured after the fifth peeling cycle (Fig. A4) show that CNTs remained attached onto the surface of pulp fibers even after being transferred to the tape surface. This demonstrates that the fortified interface between CNTs the cellulose components is greater than the adhesion strength of the tape. X-ray diffraction angles of bleached pulp handsheets prepared with various CNT:CNF ratios reveal that the crystallinity index (CrI, %) is less significantly reduced by the presence of CNTs when a specific quantity of CNF is introduced in the composite, despite the same CNT content of 15 wt% being used in each case (Fig. 1e). This result suggests that a better dispersion state with higher degree of CNT individualization is achieved at the CNT:CNF ratio of 2:1, while more compact CNT loadings are obtained both below and above this value,

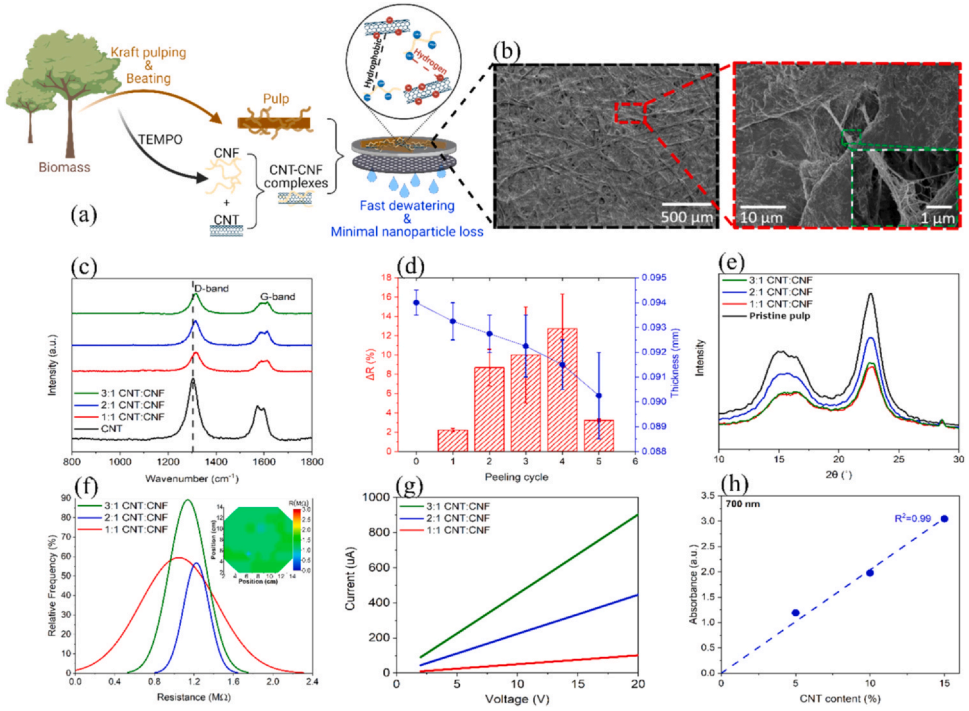

Fig. 1. Structural and electrical characterization of paper nanocomposites with 15 wt% CNT unless otherwise specified. (a) Schematic sowing the production of paper nanocomposites from renewable biomass. (b) Representative SEM micrographs of paper nanocomposites. (d) Evolution in sheet resistance and paper thickness as a function of tape peeling cycle. (c) Raman spectra, (e) X-ray diffraction patterns, (f) 4-point probe resistance measurements and (g) I-V curves of paper nanocomposites prepared at with varying CNT:CNF ratios. The inset in (f) corresponds to the spatial distribution of the electrical resistance across 37 different locations on the sheet with a 2:1 CNT:CNF ratio. (h) Optical absorption spectroscopy of papers prepared at different CNT loadings but with the same CNT:CNF ratio of 2:1.

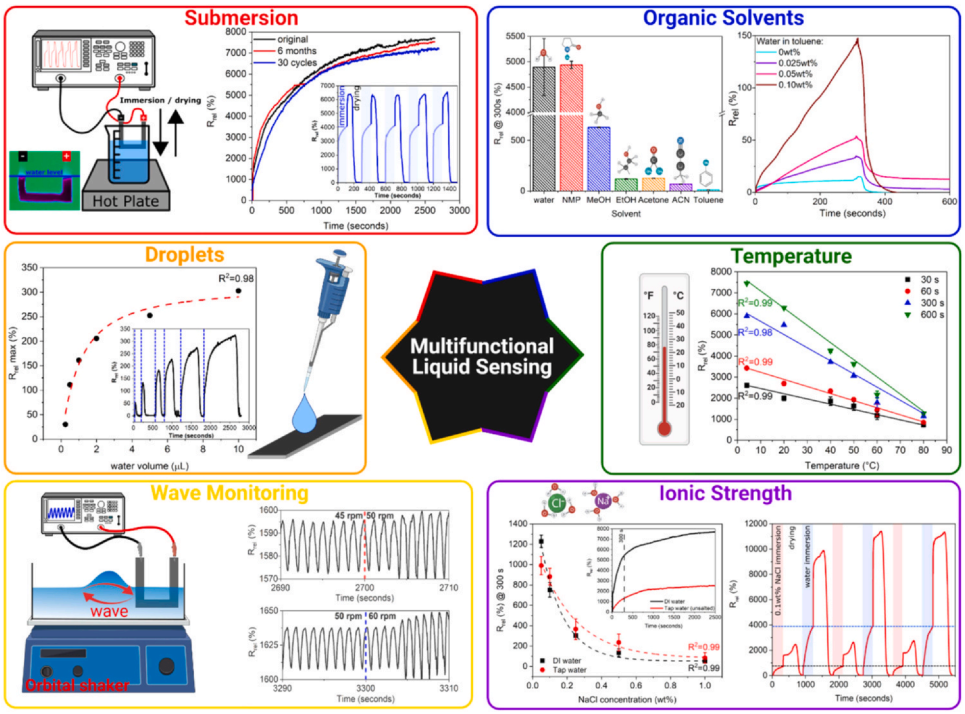

Fig. 2. Multifunctional liquid sensing performance of nanocomposites with 15 wt% and 2:1 CNT:CNF ratio. *Submersion*: The apparatus used for the submersion analysis includes thermal imaging to ensure there is no direct contact between the electrodes and the test solution (left). R_{rel} as a function of time immersed in DI water for a pristine and a 6-month aged specimen after their first and 30th immersion/drying cycle (right). The inset shows the time profile for the first 5 immersion/drying cycles. *Droplets*: The maximum R_{rel} achieved for small volumes of DI water incrementally drop casted onto the sensor (0.25, 0.5, 1, 2, 5, and 10 µL), with the corresponding time profile shown in the inset. *Wave monitoring*: R_{rel} as a function of time immersed in DI water under constant agitation using an orbital shaker successively operated at 45, 50 and 60 rpm. *Organic Solvents*: R_{rel} response at 300 s of immersion in various solvents (left) and R_{rel} time profile for different mixtures of water in toluene with increasing water content from 0.025 to 0.10 wt% (right). *Temperature*: Linear relationships of relative resistance response (R_{rel}) as a function of liquid temperature at various immersion times in DI water. *Ionic Strength*: Evolution of R_{rel} recorded at 300 s with the NaCl concentration of DI and tap water solutions, fitted with a power law (left). The inset shows the time profile in pure DI and tap water. Graph of the R_{rel} time profile over six immersion/drying cycles in alternating aqueous solutions of 0.1 wt% NaCl and pure DI water (right).

hindering the formation of crystalline regions along cellulose chains, resulting in a greater decrease in crystallinity [15,16]. This is consistent with electrical resistance measurements collected by four-point probe at 37 different locations across each sample sheet. The paper nanocomposites prepared at a CNT:CNF ratio of 2:1 yield the most uniform sheet resistance (Fig. 1f) compared to the other compositions tested (Fig. A5). Moreover, the current-voltage characteristics of paper nanocomposites exhibit a linear behavior with excellent stability and ideal Ohmic contact between the paper and the electrodes (Fig. 1g). Fig. 1h also shows that the paper absorbance is linearly proportional to the CNT content, suggesting minimal loss of nanoparticles during sheet formation and dewatering.

Multifunctional liquid sensing

Aqueous-phase sensing performance and mechanism

Paper cutouts are applied as multifunctional resistive sensors in aqueous environments, as illustrated in Fig. 2. The paper nanocomposites possess unique sensing characteristics with one of the highest sensitivity to liquid water reported (*i.e.* R_{rel}~12,000%, Fig. A6), which is defined as the ratio of the difference between the electrical resistances of the wet and dry specimen to the electrical resistance of the dry sample. Such record sensitivity enables the quantification of water volumes as small as 0.25 µL with great accuracy (Fig. 2-*droplets*). This can be attributed to the peculiar swelling behavior of cellulose in the presence of water – the diameter of pulp fibers in water increases by 28% on average compared to their original drying state (Fig. A7). While conventional sensors rely on changes in charge carrier concentration due to adsorbed water molecules, the swelling mechanism of cellulosic fibrous network allows for dramatically faster and greater responses. The presence of free water molecules can affect the interfiber spacing by disrupting hydrogen bonding between adjacent pulp fibers, although its contribution to the sheet hydroexpansion is negligible compared to the swelling of individual fibers [17–19]. Cellulose fibers are commonly understood to demonstrate two distinct swelling phases when immersed in water: an initial short but fast phase where the swelling rate reaches a maximum, followed by a longer and slower phase where the swelling rate approaches zero [20]. The resistive response of fully immersed paper sensors follows the same behavior with a steep linear increase at short times before leveling off after several minutes (Fig. 2-*submersion*). This behavior can be fitted using a pseudo second order model with correlation coefficients approaching unity (Fig. A8). The extent of cellulose expansion depends on the uptake of water molecules, which occurs mainly in the amorphous regions of cellulose where larger numbers of free hydroxyl moieties are available [20,21]. Comparing the X-ray diffractograms of dry and wet bleached and unbleached softwood pulp (Fig. A9), the same shift in the characteristic 2Θ cellulose peak is observed for both types of wet pulp (Table 1). This indicates that each sample experienced the same level of strain in their cellulose crystalline regions after soaking in water for 60 s. Despite presenting the same magnitude of expansion – in

Table 1
2D-XRD parameters for bleached and unbleached cellulose pulp, dry and after being soaked in DI water for 60 s.

Sample ID	FWHM	(200) peak 2θ (°)	CrI (%)	Crystallite size (L_{200}, nm)
Bleached dry	2.17	22.54	82.39	3.59
Bleached wet	1.89	22.72	92.74	4.12
Unbleached dry	2.26	22.51	79.64	3.45
Unbleached wet	1.93	22.72	95.09	4.03

each case the crystallite size increases by approximately 15% when wet [22], the presence of lignin in the unbleached pulp considerably limits the extent of water sorption, hence reducing the total swellable area within the sample. Besides delignification, the swellable area can be augmented further by incorporating CNFs into the paper nanocomposites as CNT dispersing agents instead of less water-swellable surfactants, creating a hierarchically swellable structure (Fig. A10a) [23–26].

The sheet density and porosity are other important factors governing the resistive response of materials to liquids [17,23]. In low density sheets, the fibers can occupy the surrounding empty space when swollen [15]. As the sheet density increases, the spacing between fibers decreases and the number of interfiber contacts increases. Therefore, there is an optimum sheet density to maximize the disruption of the percolated electrical network on the surface of individual fibers, while minimizing the reformation of CNT junctions between adjacent fibers (Fig. A10b). Finally, the CNT content and dispersion state within the fibrous network also had a strong influence on the signal response. Papers prepared with 15 wt% CNT and at a CNT:CNF ratio of 2:1 achieve the highest sensitivity to aqueous solutions due to the optimized balance between sheet resistance and CNT dispersion throughout the paper. Sharp reductions in sensitivity are observed both when the initial resistance of the paper is too high at lower CNT content, and when CNTs are less evenly distributed in the sheet due to larger quantities of hydrophobic particles in the aqueous suspension (Fig. A8).

Influence of environmental factors

Since the extent of cellulose swelling is also highly dependent upon the nature and temperature of the solvent, the paper nanocomposites can serve as liquid sensors in various applications. For instance, the fiber diameter increases by 27.5% on average when immersed in deionized water, while the radial swelling is only 7.4% in ethanol (Fig. A7). These observations are consistent with other studies and suggest that polarizability and molar volume are the main solvent characteristics influencing the swelling behavior of cellulose [13,27–30]. Based on the solvent-specific swelling response, the paper nanocomposites are not only able to distinguish between different solvents, but they can also detect the presence of water in organic solvents (Fig. 2-*organic solvents*). The detection limit is as low as 250 ppm for water in toluene, which is comparable to fluorescence methods reported in the recent literature [31], making the resistive paper sensors very compelling for the monitoring of trace water impurities during the production of fuels and chemicals. The temperature of aqueous solutions can also be measured accurately and reliably based on linear relationships between the electrical resistance and the liquid temperature with correlation coefficients approaching unity regardless of the sensing time (Fig. 2-*temperature*). The presence of ionic species in solution is another important factor influencing the resistive response of paper nanocomposites. The effect of salinity on the sensing performance is studied using sodium chloride solutions to simulate seawater (Fig. 2-*ionic strength*). Results reveal that the signal intensity decreased with the increase of salt concentration. This can be attributed to the reduced Donnan osmotic pressure between the porous paper structure and the external solution at high salt concentrations, which is caused by the ionic interactions between mobile ions and the fixed charges on the cellulosic material [20]. This result explains the different sensitivity values obtained in deionized and tap water. Furthermore, the paper nanocomposites exhibit the same predictable electrical response with correlation coefficients approaching unity when immersed in either deionized or tap water spiked with sodium chloride ranging from 0.05 to 1 wt%. Beyond this concentration range, the salt quantity is either too low or the solution conductivity is too high to yield statistically significant variations in electrical resistance. The predictable sensitivity of the paper nanocomposites to liquid temperature and salinity is especially attractive for smart aquaculture applications.

Sensing stability and cyclic analysis

Interestingly, the expansion mechanism of cellulose fibers is fully reversible, as evidenced by XRD and optical microscopy (Fig. A11). As liquid successively enters and leaves the material, the cellulose chains move apart or draw closer together, respectively. This reversible response is indicated by the elastic shift in the characteristic 2Θ cellulose peak from 22.4° to 22.2° and back as well as a reversible increase in the crystallite size from 4.5 to 4.8 nm and back. This movement is responsible for altering the electron transport by varying the intertube distance between neighbored CNTs above or below the critical tunneling distance, which is approximately 1.8 nm [13,32–34]. This translates to very reproducible sensing responses over at least 30 immersion/drying cycles (Fig. 2-*submersion*). Absorption spectroscopy also confirms the absence of individual CNT leaching in solution even when the paper sensor is immersed in water under continuous agitation for extensive periods of time up to 24 h (Fig. A12). Noteworthy, the sensor performance is not affected by aging and similar signals are obtained with the same paper-based sensor after a six-month interval. Sensing stability also remains excellent after multiple immersion/drying cycles in alternating aqueous solutions containing various levels of salts (Fig. 2-*ionic strength*). Furthermore, Laplace pressure increases as the water is withdrawn from the paper, bringing pulp fibers closer to each other due to capillary forces [35]. This rapid reorganization of the wet fibrous network contributes to fast response times, enabling applications like wave monitoring and water level measurement. The former, exemplified in Fig. 2-*wave monitoring*, shows consistent variations in the signal period with the rotation speed of the wave generator. When the rotation speed increases by 11% (*i.e.* from 45 to 50 rpm) and 20% (*i.e.* from 50 to 60 rpm), the average signal period is raised by 10% (*i.e.* from 1.22 to 1.11 s) and 19% (*i.e.* from 1.11 to 0.90 s), respectively. The latter reveals that the electrical resistance of the paper nanocomposites varied linearly with the depth of immersion, exhibiting a sensitivity of 45 $k\Omega\,mm^{-1}$ and a correlation coefficient of 0.97, as shown in Fig. A13. This implies that resistive paper sensors can monitor liquid levels in the millimeter range, which can be beneficial in various applications, such as offshore engineering constructions, overflow prevention systems and early warning of marine disasters [36,37].

Pilot scale manufacturing

In continuous flow processing, colloidal retention and dewatering time are identified as limiting factors for sheet formation [38]. Since the pore size of the wire is too large to retain the nanoparticles, filler retention is promoted by mechanical entrapment and electrostatic adsorption. First, the sheet grammage is increased from 60 to 80 $g\,m^{-2}$ and 25 wt% bleached hardwood pulp is incorporated in the paper composition to diminish the number and size of pores in the fibrous mat [39]. Then, the CNT feed is split into two filler streams of opposite charges to enhance electrostatic interactions between CNTs and pulp fibers based on our previously reported layer-by-layer nanoassembly technique [13]. The first filler addition comprises a cationic dispersion of CNTs and Cetyl Trimethyl Ammonium Bromide (CTAB 5 wt%, 2:1), which is supplied at the fan pump to ensure sufficient time and shear forces for adequate mixing with the anionic pulp. The second filler addition consisting of an aqueous mixture of CNTs and anionic lignin is introduced prior to entering the forming section (Fig. A14). As a result, the wood pulp is modified by the successive adsorption of alternating layers of oppositely charged CNTs on the surface of cellulose fibers. CNTs that are not retained in the fibrous mat during their first pass are recirculated back to the web forming section to minimize nanoparticle loss. This approach

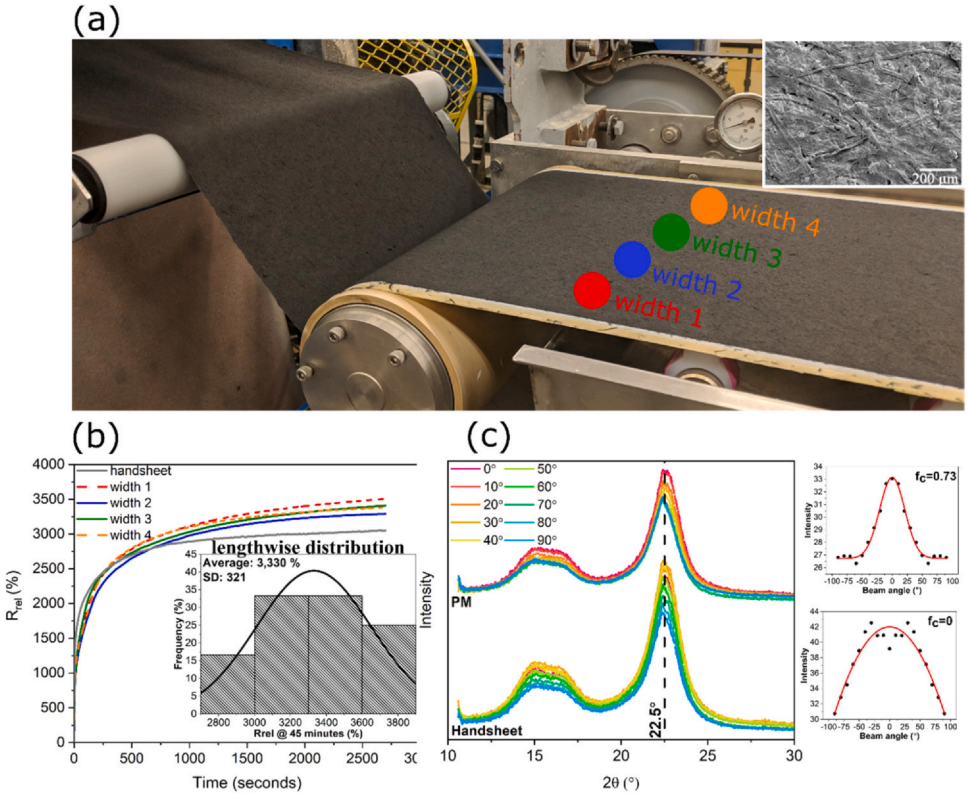

Fig. 3. Structural characterization and sensing performance of continuous flow processed paper nanocomposites: (a) Photo of the pilot-scale dynamic web forming process, with a representative SEM image of the paper nanocomposite in the inset. (b) Relative resistance response (R_{rel}) as a function of time immersed in water for samples taken across the full width (30 cm) of the sheet prepared with the dynamic web former, compared to similar samples made at the bench scale. The inset demonstrates the relatively narrow lengthwise distribution in sensitivity along the 70-m long sheet with over 35 replicates. (c) 2D-XRD profiles of paper nanocomposites produced by continuous-flow and batch scale processes, where the beam angle was rotated from 0 (in direction of continuous flow) to 90° (perpendicular to flow). The insets show the corresponding azimuthal integration of the peak at 22.5° with respect to beam angles. *Fc* values of 0.73 and 0 for the paper machine specimens (PM) and handsheets respectively, indicate some degree of fiber alignment during dynamic web formation, with *Fc* value of 1 indicating perfect alignment and *Fc* value of 0 being characteristic of randomly oriented fibrous networks.

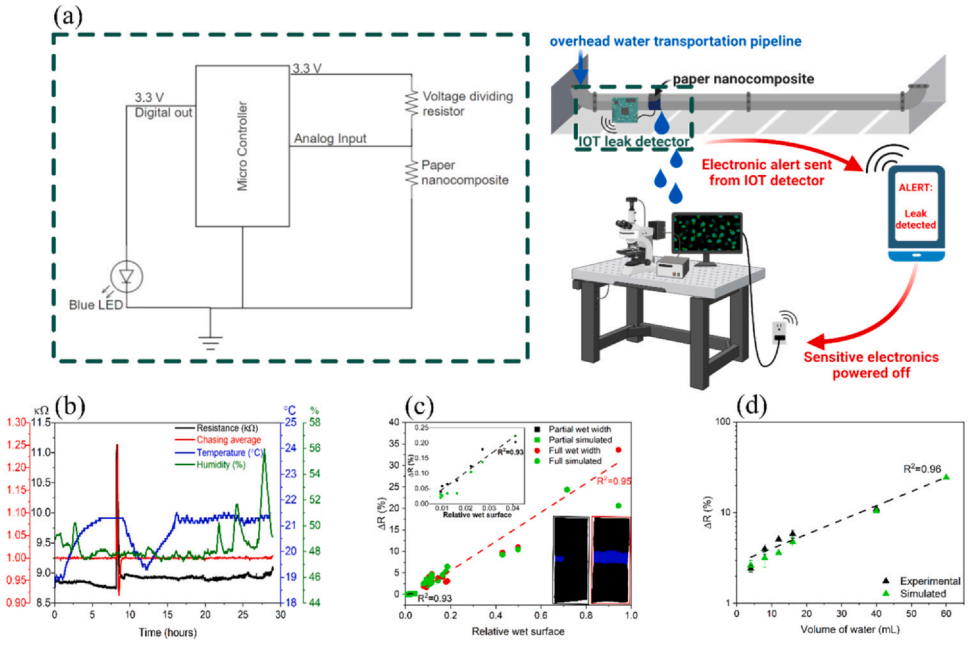

Fig. 4. Application of pilot-scale produced paper nanocomposites as remote leak detectors. (a) Schematic depicting the implementation of paper nanocomposites connected to a NodeMCU that runs an OPC UA server capable of sending alerts to the ATLAS Detector Control System upon the detection of water in an underground network of cooling pipes at the CERN facility. (b) Raw electrical resistance and processed response using a chasing average algorithm for a 30 cm × 80 cm sheet wrapped around a pipe and exposed to 0.25 mL coolant water. (c) Change in electrical resistance (ΔR) as a function of the relative wet area determined by image analysis. Inset shows expanded view of the partially wet data. (d) Change in electrical resistance (ΔR) as a function of the volume of water applied to the sheet. Simulated data points in (c) and (d) are modeled as described in ESI, where the dry unit resistance (r_d) is calibrated to equate the experimental and simulated dry sheet resistance.

yields CNT retention higher than 90% in the final sheet. Given the non-polar nature of CNTs, the dewatering was fast, enabling operating speed over 3 m min^{-1} with excellent sheet formation and uniform CNT distribution (Fig. 3a, Video A1). Paper nanocomposites with sheet dimensions of 30 cm × 80 cm are produced and exhibit homogeneous sensing performance with negligible change in sensitivity along the width and less than 10% variations along the length (Fig. 3b). Unlike batch processing, the dynamic web forming method induced the alignment of pulp fiber along the machine direction creating anisotropic sheets (*i.e.* long grain paper), as demonstrated by XRD measurements at different beam angle with the paper (Fig. 3c). While the preferred orientation of pulp fibers in the sheet has an impact on the mechanical properties (Fig. A15a), the resistive response of the paper sensor to water remains isotropic (Fig. A15b). More importantly, the signals collected from bench-scale handsheets prepared with the same characteristics (*i.e.* composition and density) are similar than those recorded with the materials made by the dynamic web former (Fig. 3b).

Supplementary material related to this article can be found online at doi:10.1016/j.nantod.2021.101270.

Leak detection applications

The paper sensors can function at low input power and do not require any active signal amplification. An inexpensive and portable leak monitoring system is developed using a NodeMCU microcontroller to send wireless text messages to a remote cellphone or computer as soon as the presence of liquid water is detected on a pipe wrapped in a paper nanocomposite sheath (Video A2). Fig. 4a depicts the prototype wiring diagram, wherein the paper nanocomposite acts as the ground-side leg in a voltage dividing circuit. When the paper gets wet, the resistance increases, causing the measured voltage to increase and triggering an alert. The leak detection system can be operated with pipes and surfaces of various nature and size by adequately adjusting the resistance threshold for triggering the alert to compensate the reduced sensitivity caused by bending or/and by contact with an electrically conductive surface (Fig. A16). Fig. 4a demonstrates how the sensory paper, when used in tandem with other Internet-of-Thing (IoT) technology, can be utilized to monitor and protect leak prone facilities by wirelessly responding to the presence of water. The rapid change in resistance within the voltage dividing circuit triggers immediate electronic alerts and allows to automatically power off sensitive electronics, preventing property damages and data losses. To mimic practical applications, the leak monitoring device is placed around a 30-cm wide section of a 13-cm diameter metallic pipe in an underground cavern of the CERN ATLAS facility and tested over a 30-h period. Water from the cooling circuit (Table A2) is drop casted (0.25 mL) on the paper sensor to simulate a leak after 8 h of testing. Fig. 4b reveals that the sub-milliliter leak is clearly identified despite fluctuations in humidity (10%) and temperature (~3 °C) using a chasing average algorithm to prevent false positives. These results demonstrate that the as-prepared leak sensors are capable of rapidly detecting the onset of water leaks the very moment it occurs to instantaneously power off sensitive instruments. Moreover, sensory papers can monitor large surfaces and be deployed in spaces with a complicated geometry by enabling 2D or 3D surface sensing, moving away from single point detection.

Supplementary material related to this article can be found online at doi:10.1016/j.nantod.2021.101270.

To explore the concept of surface detection further, the sensitivity of 30 cm × 80 cm sheets is examined as a function of the relative wet area, which is computed by image analysis of the wet samples (Fig. 4c). Two linear regimes are clearly observed depending on whether water bridges both ends of the sensor width perpendicular to the direction of the electrodes. When water completely crosses the width of the sensor, the linear resistive response exhibits a steeper slope, indicating that the paper nanocomposites are more sensitive to variations in relative wet area in the full wet width regime. In this case, the resistive signal becomes linearly proportional to the relative wet length regardless of the sensor dimensions (Fig. A17). This result is consistent with the linear relationship observed between sensitivity and depth of immersion in the fully submerged experiments (Fig. A13). On the other hand, when the sensor width was partially wet (Fig. 4c-inset), the electrical response has a lower slope and is predominantly sensitive to the relative wet width (Fig. A18). Both regimes can be modeled by dividing the paper width as a set of parallel resistors, which are linked in series along the length of the sheet. As water spreads through the paper, the value of the resistors gradually shifts from dry to wet levels, thereby increasing the equivalent resistance of the sensor. A step change is apparent when a low-resistance path through a parallel group of resistors is no longer available (*i.e.* full wet width). In this case, the equivalent resistance increases abruptly and its relationship with the wet area enters a second linear regime, where the electrical response becomes proportional to the relative wet length of the sensor. This simple model agrees very well with all experimental data as long as the sensor is not saturated with water, which happens when the relative wet surface approaches unity. At this point, the simulation underestimates the resistive signal. Furthermore, the electrical response at a given relative wet area is also correlated with the volume of water, as demonstrated by both experimental and simulation data (Fig. 4d). This work provides a framework for the quantification of various liquids over large surfaces, which bears important implications for the sustainable and efficient management of fluids. Finally, there are no statistical differences in resistance when the relative wet area is computed either from multiple discrete small wet spots or from a single wet spot of larger dimensions (Fig. A19a). Similarly, no statistical differences are observed between data collected with a single strip of paper sensor and data obtained from a specimen of the same size but comprising multiple strips connected to each other with aluminum tape (Fig. A19b). This means that paper nanocomposites can be cut and reattached easily using conductive tape without altering their sensing performance. Their versatility combined with their innate flexibility makes it possible to design sensory papers with nearly every imaginable shapes for various applications in buildings, distribution lines, household manifolds, miniaturized cooling pipes and mobile tanks in ships and trucks.

Conclusion

In summary, the use of paper nanocomposites as leak detectors for aqueous and organic solvents is very promising, due to the combined technological and economic benefits. The tailored and cost-efficient web forming process is based on mature industrial systems, allowing the transfer of laboratory scale sensors to commercial applications. Low-cost arrays of highly sensitive and responsive liquid sensing devices can be deployed over large areas, in inaccessible spaces, and challenging configurations, to mitigate liquid damages and reduce utility bills by rapidly powering off sensitive instruments and locating leaks.

Experimental method

Batch-scale preparation

Paper nanocomposites are prepared by combining pulp fibers (WestRock Company and Boise Cascade) with aqueous suspensions of hydroxyl-functionalized CNTs (Cheap Tubes Inc., 0.7% OH) and TEMPO-oxidized cellulose nanofibrils (CNFs), dispersed using a double acoustic irradiation system prior to sheet formation [13,40]. For comparison purposes, helical CNTs and graphene nanoplatelets

purchased from Cheap Tubes Inc. were also used as conductive fillers. The modified pulp is then filtered through a handsheet mold (Essex International Inc. custom machinery), and pressed and dried according to TAPPI T-205 standards [13]. The quantities of pulp, CNTs, and CNF are adjusted to control the resulting composite density and porosity, and maintain final CNT contents of either 5, 10, or 15 wt%.

Pilot-scale manufacturing

Paper comprising a blend of cellulose fibers from softwood and hardwood (75:25) sources is produced using a 32-cm wide dynamic sheet former (Noble and Wood) operated at 3.2 m min^{-1}. Prior to sheet formation, the pulp is alternatingly dosed with two aqueous dispersions of CNTs pre-absorbed with oppositely charged surfactants, namely CTAB (5 wt%, 2:1) and alkali lignin (5 wt%, 2:1). The CNT loading in the final sheet is set to ~18 ± 2 wt% by adjusting the injection flow rate of each CNT dispersion. Dewatering is achieved by subsequent pressing at 50 PSIG and drying at 80 °C. The resulting paper nanocomposite is wrapped around a 10-cm diameter roll before being unwind and cut into sheets of 30 cm × 80 cm using an automated sheet slicer (Kunshan Dapeng Precision Machinery Co., Ltd., DP-360CQ).

Structural and electrical characterization

The paper morphology is characterized by SEM. Raman spectroscopy and tape peeling tests are conducted to analyze the interfacial properties of the fibrous composites. The hygroexpansion of the paper sensors is investigated by optical microscopy and XRD. Optical absorption spectroscopy is employed to assess the CNT distribution and retention during sheet formation. The electrical properties are examined based on current-voltage (I-V) characteristics and 4-point probe measurements.

Sensing performance

Liquid water sensing measurements are performed using a Keithley 2450 voltage-current meter to monitor changes in electrical resistance across cutouts from the as-prepared paper nanocomposites when either immersed in solution or wetted *via* drop-casting small volumes onto the paper surface. Sensing performance is quantified based on the relative resistance (R_{rel}), defined as the ratio of the difference between the electrical resistances of the wet and dry specimen to the electrical resistance of the dry sample. When utilized in a portable leak monitoring system, the paper nanocomposite was wired in series with a resistor ohm matched to its dry state, creating a voltage-dividing circuit. A NodeMCU microcontroller supplied the input voltage and sampled the output voltage from the voltage-dividing circuit, wirelessly relaying a message to the If This Then That (IFTTT) webhook service to facilitate device-to-device communication.

CRediT authorship contribution statement

S.M. Goodman: Methodology, Investigation, Data curation, Visualization, Writing – Original draft preparation. **I. Asensi Tortajada:** Methodology, Investigation, Data curation, Software. **Florian Haslbeck**: Formal analysis, Investigation, Data curation. **K.Y. Oyulmaz:** Investigation, Data curation. **A. Rummler:** Validation, Supervision, Resources. **C. Solans Sánchez:** Validation, Supervision, Resources, Writing – Reviewing and Editing. **J. Torres País:** Supervision. **H. Denizli:** Supervision. **K.J. Haunreiter:** Resources. **A.B. Dichiara:** Conceptualization, Supervision, Funding acquisition, Project administration, Resources, Writing – Reviewing and Editing.

Declaration of Competing Interest

The authors declare that they have no known competing financial interests or personal relationships that could have appeared to influence the work reported in this paper.

Acknowledgments

This research is supported by the Advanced Manufacturing Program (No. 1927623) from the National Science Foundation and by the McIntire-Stennis Cooperative Forestry Research Program (No. 1020630) from the USDA National Institute of Food and Agriculture. The authors also thank WestRock Paper Company for donated the wood pulp used in this research. Open access funding is enabled and organized by CERN.

Appendix A. Supporting information

Supplementary data associated with this article can be found in the online version at doi:10.1016/j.nantod.2021.101270.

References

[1] Drinking Water Report, ASCEs 2017 Infrastruct. Rep. Card., 2019. ⟨https://www.infrastructurereportcard.org/cat-item/drinking_water/⟩ (accessed 10 April 2019).
[2] O. US EPA, Fix a Leak Week, US EPA, 2017. ⟨https://www.epa.gov/watersense/fix-leak-week⟩ (accessed 23 December 2019).
[3] K. Parikh, K. Cattanach, R. Rao, D.-S. Suh, A. Wu, S.K. Manohar, Flexible vapour sensors using single walled carbon nanotubes, Sens. Actuators B Chem. 113 (2006) 55–63, https://doi.org/10.1016/j.snb.2005.02.021
[4] J.A. Covington, J.W. Gardner, D. Briand, N.F. de Rooij, A polymer gate FET sensor array for detecting organic vapours, Sens. Actuators B Chem. 77 (2001) 155–162, https://doi.org/10.1016/S0925-4005(01)00687-6
[5] J. Barkauskas, Investigation of conductometric humidity sensors, Talanta 44 (1997) 1107–1112, https://doi.org/10.1016/S0039-9140(96)02203-5
[6] A. Bouvree, J.-F. Feller, M. Castro, Y. Grohens, M. Rinaudo, Conductive Polymer nano-bioComposites (CPC): Chitosan-carbon nanoparticle a good candidate to design polar vapour sensors, Sens. Actuators B Chem. 138 (2009) 138–147, https://doi.org/10.1016/j.snb.2009.02.022
[7] T. Villmow, S. Pegel, A. John, R. Rentenberger, P. Pötschke, Liquid sensing: smart polymer/CNT composites, Mater. Today 14 (2011) 340–345, https://doi.org/10.1016/S1369-7021(11)70164-X
[8] X. Wu, Y. Han, X. Zhang, C. Lu, Hierarchically structured composites for ultrafast liquid sensing and smart leak-plugging, Phys. Chem. Chem. Phys. 19 (2017) 16198–16205, https://doi.org/10.1039/C7CP02293J
[9] N. Kurra, G.U. Kulkarni, Pencil-on-paper: electronic devices, Lab. Chip 13 (2013) 2866–2873, https://doi.org/10.1039/C3LC50406A
[10] T.H. da Costa, E. Song, R.P. Tortorich, J.-W. Choi, A paper-based electrochemical sensor using inkjet-printed carbon nanotube electrodes, ECS J. Solid State Sci. Technol. 4 (2015) S3044–S3047, https://doi.org/10.1149/2.0121510jss
[11] O.-S. Kwon, H. Kim, H. Ko, J. Lee, B. Lee, C.-H. Jung, J.-H. Choi, K. Shin, Fabrication and characterization of inkjet-printed carbon nanotube electrode patterns on paper, Carbon 58 (2013) 116–127, https://doi.org/10.1016/j.carbon.2013.02.039
[12] L. Hu, J.W. Choi, Y. Yang, S. Jeong, F. La Mantia, L.-F. Cui, Y. Cui, Highly conductive paper for energy-storage devices, Proc. Natl. Acad. Sci. USA 106 (2009) 21490–21494, https://doi.org/10.1073/pnas.0908858106
[13] A.B. Dichiara, A. Song, S.M. Goodman, D. He, J. Bai, Smart papers comprising carbon nanotubes and cellulose microfibers for multifunctional sensing applications, J. Mater. Chem. A 5 (2017) 20161–20169, https://doi.org/10.1039/C7TA04329E
[14] A. Hajian, S.B. Lindström, T. Pettersson, M.M. Hamedi, L. Wågberg, Understanding the dispersive action of nanocellulose for carbon nanomaterials, Nano Lett. 17 (2017) 1439–1447, https://doi.org/10.1021/acs.nanolett.6b04405
[15] S. Bi, L. Hou, H. Zhao, L. Zhu, Y. Lu, Ultrasensitive and highly repeatable pen ink decorated cuprammonium rayon (cupra) fabrics for multifunctional sensors, J. Mater. Chem. A 6 (2018) 16556–16565, https://doi.org/10.1039/C8TA04809F
[16] S. Zhang, F. Zhang, Y. Pan, L. Jin, B. Liu, Y. Mao, J. Huang, Multiwall-carbon-nanotube/cellulose composite fibers with enhanced mechanical and electrical properties by cellulose grafting, RSC Adv. 8 (2018) 5678–5684, https://doi.org/10.1039/C7RA11304H
[17] A.T. Jafry, H. Lim, S.I. Kang, J.W. Suk, J. Lee, A comparative study of paper-based microfluidic devices with respect to channel geometry, Colloids Surf. Physicochem. Eng. Asp. 492 (2016) 190–198, https://doi.org/10.1016/j.colsurfa.2015.12.033
[18] H. Qi, B. Schulz, T. Vad, J. Liu, E. Mäder, G. Seide, T. Gries, Novel carbon nanotube/cellulose composite fibers as multifunctional materials, ACS Appl. Mater. Interfaces 7 (2015) 22404–22412, https://doi.org/10.1021/acsami.5b06229

[19] P.A. Larsson, L. Wågberg, Diffusion-induced dimensional changes in papers and fibrillar films: influence of hydrophobicity and fibre-wall cross-linking, Cellulose 17 (2010) 891–901, https://doi.org/10.1007/s10570-010-9433-7
[20] M. Botková, Š. Šutý, M. Jablonský, L. Kucerkova, M. Vrška, Monitoring of kraft pulps swelling in water, Cell. Chem. Technol. 47 (2013) 95–102.
[21] H. Qi, E. Mäder, J. Liu, Unique water sensors based on carbon nanotube–cellulose composites, Sens. Actuators B Chem. 185 (2013) 225–230, https://doi.org/10.1016/j.snb.2013.04.116
[22] M. Agarwal, Q. Xing, B.S. Shim, N. Kotov, K. Varahramyan, Y. Lvov, Conductive paper from lignocellulose wood microfibers coated with a nanocomposite of carbon nanotubes and conductive polymers, Nanotechnology 20 (2009) 215602, https://doi.org/10.1088/0957-4484/20/21/215602
[23] Y. Qing, Y. Wu, Z. Cai, X. Li, Water-triggered dimensional swelling of cellulose nanofibril films: instant observation using optical microscope, J. Nanomater. 2013 (2013) 1–6, https://doi.org/10.1155/2013/594734
[24] S. Fält, L. Wågberg, E.-L. Vesterlind, Swelling of model films of cellulose having different charge densities and comparison to the swelling behavior of corresponding fibers, Langmuir 19 (2003) 7895–7903, https://doi.org/10.1021/la026984i
[25] V. Ottesen, K. Syverud, Swelling of individual cellulose nanofibrils in water, role of crystallinity: an AFM study, Cellulose 28 (2021) 19–29, https://doi.org/10.1007/s10570-020-03517-8
[26] V. Ottesen, P.T. Larsson, G. Chinga-Carrasco, K. Syverud, Ø.W. Gregersen, Mechanical properties of cellulose nanofibril films: effects of crystallinity and its modification by treatment with liquid anhydrous ammonia, Cellulose 26 (2019) 6615–6627, https://doi.org/10.1007/s10570-019-02546-2
[27] O.A. El Seoud, L.C. Fidale, N. Ruiz, M.L.O. D'Almeida, E. Frollini, Cellulose swelling by protic solvents: which properties of the biopolymer and the solvent matter? Cellulose 15 (2008) 371–392, https://doi.org/10.1007/s10570-007-9189-x
[28] G.I. Mantanis, R.A. Young, R.M. Rowell, Swelling of compressed cellulose fiber webs in organic liquids, Cellulose 2 (1995) 1–22, https://doi.org/10.1007/BF00812768
[29] A.A. Robertson, Cellulose-Liquid Interactions, Pulp Pap. Mag. Can. (1964) 171–178.
[30] A.A. Robertson, Interactions of liquids with cellulose, TAPPI 53 (1970) 1331–1339.
[31] P. Yuvaraj, J. Ajantha, S. Easwaramoorthi, J. Raghava Rao, Low-level detection of water in polar aprotic solvents using an unusually fluorescent spirocyclic rhodamine, N. J. Chem. 44 (2020) 6566–6574, https://doi.org/10.1039/D0NJ00636J
[32] Alamusi, N. Hu, H. Fukunaga, S. Atobe, Y. Liu, J. Li, Piezoresistive strain sensors made from carbon nanotubes based polymer nanocomposites, Sensors 11 (2011) 10691–10723, https://doi.org/10.3390/s111110691
[33] P. Verma, M.L. Shofner, A.C. Griffin, Deconstructing the auxetic behavior of paper, Phys. Status Solidi B 251 (2014) 289–296, https://doi.org/10.1002/pssb.201384243
[34] C. Li, E.T. Thostenson, T.-W. Chou, Dominant role of tunneling resistance in the electrical conductivity of carbon nanotube–based composites, Appl. Phys. Lett. 91 (2007) 223114, https://doi.org/10.1063/1.2819690
[35] A. Tejado, T.G.M. van de Ven, Why does paper get stronger as it dries? Mater. Today 13 (2010) 42–49, https://doi.org/10.1016/S1369-7021(10)70164-4
[36] B.D. Chen, W. Tang, C. He, C.R. Deng, L.J. Yang, L.P. Zhu, J. Chen, J.J. Shao, L. Liu, Z.L. Wang, Water wave energy harvesting and self-powered liquid-surface fluctuation sensing based on bionic-jellyfish triboelectric nanogenerator, Mater. Today 21 (2018) 88–97, https://doi.org/10.1016/j.mattod.2017.10.006
[37] M. Xu, S. Wang, S.L. Zhang, W. Ding, P.T. Kien, C. Wang, Z. Li, X. Pan, Z.L. Wang, A highly-sensitive wave sensor based on liquid-solid interfacing triboelectric nanogenerator for smart marine equipment, Nano Energy 57 (2019) 574–580, https://doi.org/10.1016/j.nanoen.2018.12.041
[38] D.O. Castro, Z. Karim, L. Medina, J.-O. Häggström, F. Carosio, A. Svedberg, L. Wågberg, D. Söderberg, L.A. Berglund, The use of a pilot-scale continuous paper process for fire retardant cellulose-kaolinite nanocomposites, Compos. Sci. Technol. 162 (2018) 215–224, https://doi.org/10.1016/j.compscitech.2018.04.032
[39] B. Nordström, Effects of grammage on paper properties for twin-wire roll forming of TMP, J. Pulp Pap. Sci. 21 (1995) 427–431.
[40] S.M. Goodman, N. Ferguson, A.B. Dichiara, Lignin-assisted double acoustic irradiation for concentrated aqueous dispersions of carbon nanotubes, RSC Adv. 7 (2017) 5488–5496, https://doi.org/10.1039/C6RA25986C